Atomic structure of the unique antiferromagnetic 2/1 quasicrystal approximant

Farid Labib,[1] Hiroyuki Takakura,[2] Asuka Ishikawa,[3] and Ryuji Tamura[1]
[1]*Department of Materials Science and Technology, Tokyo University of Science, Tokyo 125-8585, Japan*
[2]*Division of Applied Physics, Faculty of Engineering, Hokkaido University, Sapporo 060-8628, Japan*
[3]*Research Institute of Science and Technology, Tokyo University of Science, Tokyo 125-8585, Japan*

(Received 12 July 2022; accepted 26 April 2023; published 15 May 2023)

The atomic structure of the recently discovered antiferromagnetic (AFM) $Ga_{50}Pd_{35.5}Tb_{14.5}$ 2/1 approximant to quasicrystal with the space group of $Pa\bar{3}$ (No. 205), $a = 23.1449(0)$ Å was determined by means of single-crystal x-ray diffraction. The refined structure model revealed two main building units, namely, a Tsai-type rhombic triacontahedron (RTH) cluster with three concentric inner shells and an acute rhombohedron filling the gaps in between the RTH clusters. One of the interesting findings was a very low number of chemically mixed sites in the structure, which amount to only 7.40% of the all the atomic sites within an RTH cluster. A disorder-free environment was noticed within a nearest neighbor of an isolated Tb^{3+} ion, which is presumably one of the main contributors in enhancing AFM order in the present compound. The second significant finding was the observance of an orientationally ordered trigonal pyramidlike unit with a height of 4.2441(7) Å at the center of the RTH cluster. Such a unit is noticed to bring structural distortion to outer shells, particularly to the surrounding dodecahedron cage being another possible contributor to the AFM order establishment in the present compound. The results, therefore, are suggestive of a possible link between chemical/positional order and the AFM order establishment.

DOI: 10.1103/PhysRevB.107.184110

I. INTRODUCTION

Icosahedral quasicrystals (*i*QCs), as aperiodically ordered intermetallic compounds, generate sharp Bragg reflections with fivefold rotational symmetry forbidden to crystals, indicating the presence of long-range order without periodicity in their atomic configuration [1]. Among various types of classified quasicrystals (QCs), namely, the Mackay- [2,3], Bergman- [4,5], and Tsai-type [6–8], the latter is the most abundant type to date. An accurate structure analysis of the *i*QC has been attained in the binary $Cd_{5.7}Yb$ compound [9], thanks to its high structural quality without chemical disorder, which revealed two main building units in the structure: a multishell polyhedron, as demonstrated in Fig. 1(a), with four concentric shells (from the outermost one): a rhombic triacontahedron (RTH), an icosidodecahedron, an icosahedron, and a dodecahedron caging a central tetrahedron. Within the RTH cluster, the rare-earth (RE) elements exclusively occupy the vertices of an icosahedron. The second building unit is an acute rhombohedron (AR) which fills the gaps between the RTH clusters and accommodates two additional RE elements on its long body diagonal axis.

Approximant crystals (ACs), as crystalline counterparts of *i*QCs, encompass the same building units of *i*QCs being arranged periodically with translational symmetry [10]. The term AC is commonly preceded by a rational approximation f_{n+1}/f_n of τ defined as $(1+\sqrt{5})/2$, with f_n representing the nth Fibonacci number. In this scheme, the higher the rational approximation we take, the more the structure resemblances to that of an *i*QC [10]. The binary $Cd_{5.7}Yb$ *i*QC [9], $Cd_{76}Yb_{13}$ 2/1 AC [11], and Cd_6Yb 1/1 AC [6] are usually believed to be prototype Tsai-type compounds from which a large number of ternary or even quaternary and quinary *i*QCs and ACs have been discovered [12–18] by simply replacing Cd with other metallic species and Yb with various RE elements.

As far as their atomic structures are concerned, in the 1/1 AC, which can be described as a body-centered cubic packing of RTH clusters with the space group $Im\bar{3}$ [19], the AR unit is absent, and the central tetrahedra rarely resembles that shown in Fig. 1(a). Rather, it exhibits at least one of the two classified disorder types shown in Fig. 1(b), i.e., types I and II, which refer to a 90 ° rotation of the tetrahedron along its twofold axis and a positional splitting of the tetrahedron vertices, respectively [19]. There are some exceptions such as $Cd_{37}Ce_6$ [20], $(Cd, Mg)_{37}Ce_6$ [21], $Cd_{25}Eu_4$ [22], and $(Cd, Mg)_{25}Ce_4$ [21] 1/1 ACs, though, where the tetrahedrons are orientationally ordered with different fashions lowering the symmetry from $Im\bar{3}$ to $Pn\bar{3}$ in the two former cases and to $Fd\bar{3}$ in the two latter. It is also worth noting that the binary Cd_6RE (RE = Y, Sm, Gd, Tb, Dy, Ho, Er, and Tm) 1/1 ACs undergo structural transition below specific temperatures (depending on the RE type) where the disordered central tetrahedra become orientationally fixed [23]. Whether such structural transition takes part in development of long-range antiferromagnetic (AFM) order in the same compounds [24,25] is still an open question. In some alloy systems, referred to as pseudo-Tsai-type systems, on the other hand, 1/1 ACs encompass a single fully or partially occupied RE element at the center of the RTH cluster instead of a tetrahedron [26,27].

Despite a profound knowledge attained about the structural characteristics of the 1/1 ACs in the last two decades, little is known about the structure of their higher-order counterparts such as 2/1 ACs. This might be partly related to the fact that 2/1 ACs are not as abundant as 1/1 ACs when it

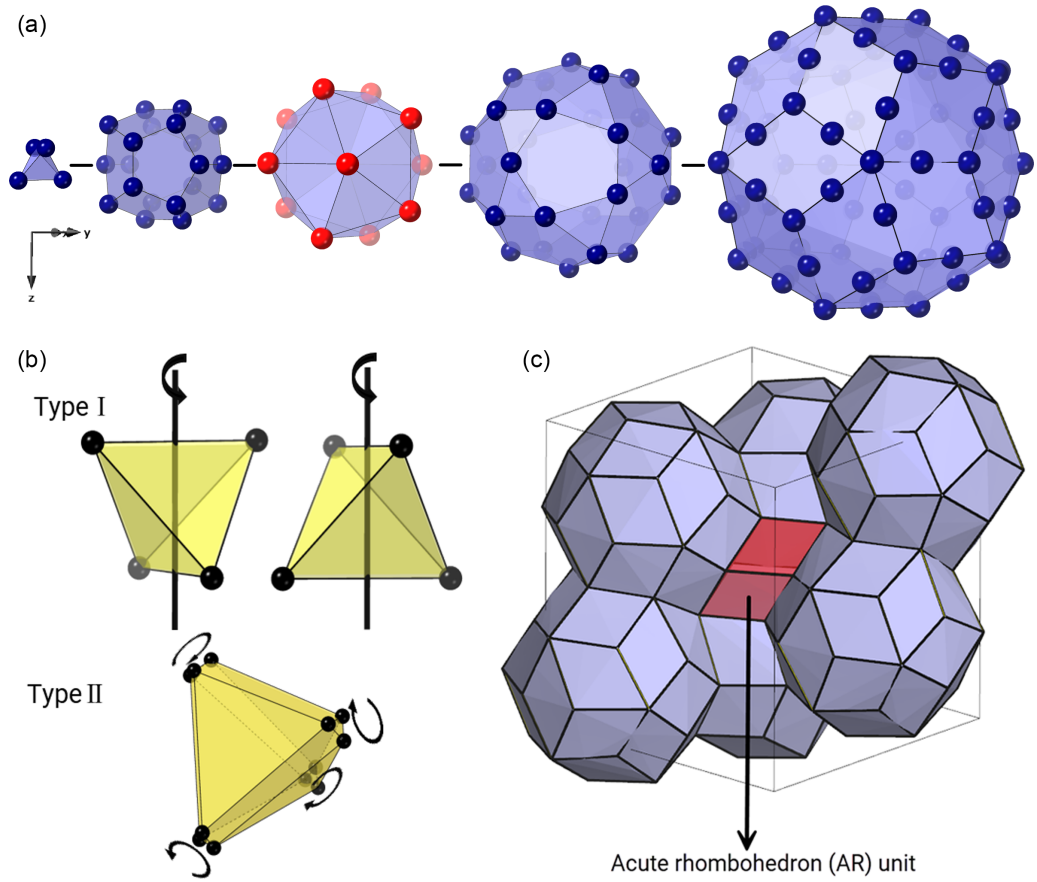

FIG. 1. (a) A typical shell structure of the Tsai-type icosahedral quasicrystal (*i*QC) in Cd-Yb system. From center to outermost shell: inner Cd tetrahedron (4 atoms), Cd dodecahedron (20 atoms), Yb icosahedron (12 atoms), Cd icosidodecahedron (30 atoms), and Cd rhombic triacontahedron (RTH; 92 atoms). (b) Type I and II disorders of the central tetrahedron with the former corresponding to the orientational rotation of a tetrahedron by 90° with respect to twofold axes and the latter being triple splitting of the tetrahedron vertices. (c) Typical arrangement of RTH clusters within one unit cell in the 2/1 approximant crystal (AC) including an acute rhombohedron (AR) that fills the gap between the RTH clusters.

comes to their formation in the phase diagram. The structure of these compounds, which crystallize in the space group of $Pa\bar{3}$ [9], closely resembles that of *i*QCs (space group: $Pm\bar{3}5$ [9]), e.g., both comprise RTH and AR units as their main building units. Figure 1(c) provides a schematic view of the AR unit within a typical 2/1 AC unit cell. Based on two reports [11,28], the orientation of the innermost core unit in the 2/1 AC no longer follows the disorder modes described in Fig. 1(b). Rather, three elongated arc-shaped electron density distributions, roughly resembling a trigonal bipyramid, are noticed and explained by off-center displacement of the central tetrahedron. In one of the latest efforts in this regard [28], the atomic structure of the Cd-Mg-Y 2/1 AC has been examined, and high levels of chemical disorder between the Cd and Mg species were noticed in most of the atomic sites.

In this paper, therefore, we aim to carefully examine the structural parameters of the Ga-Pd-Tb 2/1 AC by means of single-crystal x-ray diffraction (SCXRD). This compound is of special interest due to several reasons. It is the only reported ternary non-Au-based Tsai-type compound that exhibits long-range AFM order at low temperatures [29,30]. Moreover, unlike the rest of the reported AFM ACs to date, this compound has high electron-per-atom density ($e/a = 1.93$) under the assumption of Ga and Pd being trivalent and zerovalent, respectively. More importantly, it is one of the two reported 2/1 ACs with AFM order (the other one being $Au_{65}Ga_{20}Eu_{15}$ 2/1 AC with $e/a = 1.54$), the structure of which, in principle, contains all necessary components to construct an *i*QC. These points further necessitate structural determination of the present compound, the outcome of which should deepen our understanding about not only the atomic structure of high-order ACs but also their structural link with corresponding *i*QCs, especially around the cluster center. It should also shed light on the unique AFM order observed at low temperatures and guide the quest for finding the AFM *i*QC in the future, which is attainable based on several theoretical studies [31–37] but yet to be discovered experimentally.

II. EXPERIMENT

Polycrystalline alloy with a nominal composition of $Ga_{50}Pd_{35.5}Tb_{14.5}$ was synthesized from high-purity Ga (99.9999 wt. %), Pd (99.95 wt. %), and Tb (99.9 wt. %) elements using an arc-melting technique. The synthesized sample was then heat treated at 973 K under an Ar atmosphere for 120 h followed by water quenching. Powder x-ray diffrac-

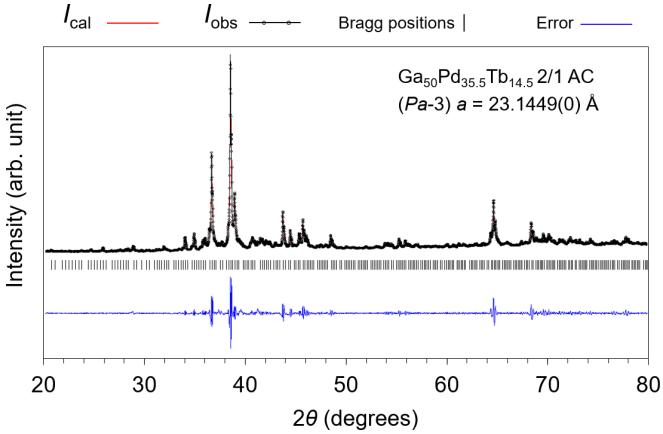

FIG. 2. Le Bail fitting of powder x-ray diffraction (XRD) pattern of the $Ga_{50}Pd_{35.5}Tb_{14.5}$ 2/1 approximant crystal (AC) annealed at 973 K.

tion (XRD) was carried out for phase identification using a Rigaku SmartLab SE x-ray diffractometer with Cu-$K\alpha$ radiation. For structural determination, a piece of single crystal of $\sim 0.02 \times 0.03 \times 0.03\ \text{mm}^3$ in size was extracted from the sample and examined using laboratory XRD. The SCXRD data were collected at room temperature using a Rigaku XtaLAB Synergy-R single-crystal diffractometer with a rotating anode Mo-$K\alpha$ x-ray source. An initial structure model was obtained successfully by using SHELXT [38]. Subsequent structure refinements were conducted using SHELXL [39].

III. RESULTS

Figure 2 represents the powder XRD pattern and Le Bail fitting of the synthesized $Ga_{50}Pd_{35.5}Tb_{14.5}$ compound after an isothermal annealing at 973 K for 120 h [40]. The fitting curve was obtained by assuming the space group $Pa\bar{3}$ using the JANA 2020 software suite [41]. The red, black, and blue lines in the figure represent calculated (I_{cal}) and measured (I_{obs}) peak intensities and the difference between them, respectively, while the black vertical bars indicate expected Bragg peak positions. As shown, there is fair agreement between the experimental and calculated peak positions and intensities, confirming high purity of the synthesized 2/1 AC. Figure 3 illustrates the reciprocal-space sections perpendicular to the [100], [110], [11$\bar{1}$], and [850] zone axes, obtained from SCXRD data after reconstruction. In total, 351 711 Bragg reflections are noticed with a resolution limit equal to ~0.8 Å. The data reduction is performed by assuming the space group $Pa\bar{3}$ (No. 205) leading to 5875 unique reflections and a converged reliability factor of $R\ [F^2 > 2\sigma(F^2)] = 0.0383$. The $wR(F^2)$, with w defined as $1/[\sigma(F_{abs}^2)^2 + (0.0026P)^2 + 217.66P]$, equals 0.0450 for all reflections with positive intensities, and the goodness of fit S is 1.383. The composition of the refined model $Ga_{50.3}Pd_{35.7}Tb_{14.0}$ is in good agreement with the measured composition $Ga_{50.21}Pd_{35.48}Tb_{14.31}$ obtained from inductively coupled plasma atomic emission spectroscopy (ICP-AES) analysis. The crystallographic data for the refined structure are listed in Table I. No significant violation of the systematic extinction rule for $Pa\bar{3}$ (i.e., $0kl$: $k = 2n$, $h00$: $h = 2n$) is noticed. Table II lists atomic coordinates, Wyckoff positions, site occupations, and equivalent isotropic displacement parameters (U_{eq}) after refinement.

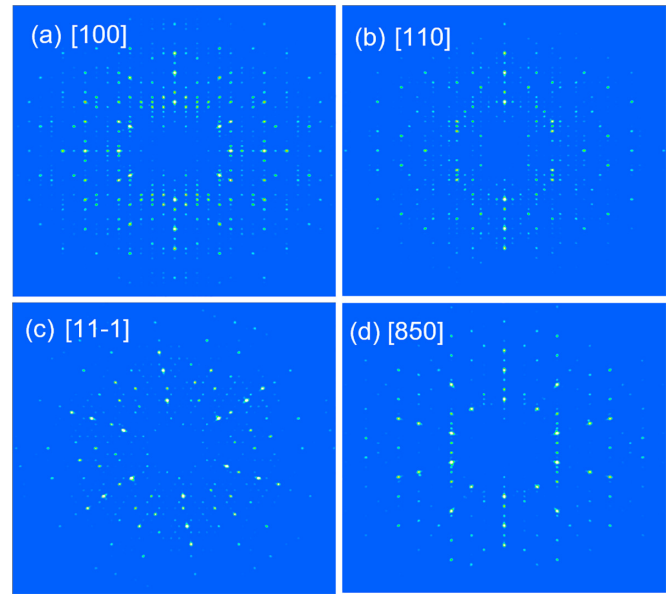

FIG. 3. Constructed reciprocal space sections perpendicular to (a) [110], (b) [110], (c) [11-1], and (d) [850] directions of the $Ga_{50}Pd_{35.5}Tb_{14.5}$ 2/1 approximant crystal (AC).

Figure 4(a) presents the final refined structure model within a unit cell with a lattice parameter of 23.1449(0) Å viewed along the [100] direction where Ga, Pd, and Tb atoms and unoccupied sites are represented by blue, green, red, and white spheres, respectively. Figure 4(b) illustrates the concentric atomic shells that constitute one RTH cluster. As a common

TABLE I. Crystallographic data for the refined structure.

Chemical formula	$Ga_{372.09}\ Pd_{264.13}\ Tb_{104}$
Molar mass M_r	69 409.07
Temperature of data collection (K)	298
Space group	$Pa\bar{3}$ (No. 205)
a axis (Å)	23.1449(0)
Cell volume (Å^3)	12 398.408
Z	1
$F(000)$	29 935
Calculated density (g/cm^3)	9.4518
Radiation type	Mo $K\alpha$
Absorption coefficient (mm^{-1})	43.089
Crystal size (mm^3)	0.02×0.03×0.03
2θ range (deg.)	3.293 − 25.242
No. of measured, independent, and observed $[I > 2\sigma(I)]$ reflections	351 711, 6319, 5875
R_{int}	0.0441
No. of parameters	367
No. of restrains	0
$R[F2 > 2\sigma(F^2)]$, $wR(F^2)$, S	0.0383, 0.0450, 1.383
Absorption correction	Gaussian integration
T_{min}, T_{max}	0.358, 0.479
$\Delta\rho_{min}$, $\Delta\rho_{max}$ (e/Å^3)	−1.297, 1.539

TABLE II. Atomic coordinates, Wyckoff position, site occupation, and equivalent isotropic displacement parameter ($U_{eq.}$) after refinement.

Unit/shell	Atom	Site	Wyckoff position	x	y	z	Occupation	U_{eq}(Å)^2
Central unit	Ga	G_1	8*c*	0.0955(3)	0.0955(3)	0.0955(3)	1	0.0100(2)
	Ga	G_2	24*d*	0.15256(4)	0.19301(4)	0.25855(5)	0.953(6)	0.0131(4)
	Pd	P_2	24*d*	0.1704(14)	0.1752(14)	0.2413(13)	0.027(4)	0.021(9)
	Ga	$Ga_{dis.1}$	24*d*	0.10364(17)	0.18724(9)	0.15696(9)	0.526(3)	0.0084(9)
	Ga	$Ga_{dis.2}$	24*d*	0.0756(3)	0.18645(18)	0.1727(2)	0.315(11)	0.0169(17)
	Ga	$Ga_{dis.3}$	24*d*	0.08710(13)	0.13046(16)	0.19707(13)	0.274(2)	0.0145(14)
	Ga	$Ga_{dis.4}$	24*d*	0.09006(17)	0.2109(2)	0.1307(3)	0.241(7)	0.030(2)
	Ga	$Ga_{dis.5}$	24*d*	0.0928(13)	0.1657(18)	0.1844(13)	0.079(10)	0.053(9)
Dodecahedron	Pd	P1	8*c*	0.1533(17)	0.1533(17)	0.1533(17)	0.017(6)	0.02(2)
	Pd	P_5	8*c*	0.03558(2)	0.03558(2)	0.03558(2)	1	0.01092(17)
	Pd L[a]	P_6	24*d*	0.15615(3)	0.23196(3)	0.35998(3)	0.965(4)	0.0178(2)
	Pd	P_7	24*d*	0.00049(2)	0.15689(2)	0.09776(2)	1	0.01131(10)
	Pd	P_8	24*d*	0.09308(2)	0.30819(2)	0.15185(2)	1	0.01308(11)
	Pd	P_9	24*d*	0.05458(2)	0.24717(3)	0.25103(3)	0.975(2)	0.01405(19)
	Pd	P_{10}	24*d*	0.15615(3)	0.23196(3)	0.35998(3)	0.965(4)	0.018(2)
	Ga	G_{10}	24*d*	0.1520(10)	0.2216(10)	0.3274(13)	0.034(5)	0.008(8)
	Ga	G_4	24*d*	0.15362(10)	0.27944(11)	0.48278(14)	0.685(3)	0.0081(4)
	Pd	P_4	24*d*	0.15401(17)	0.2879(2)	0.5048(4)	0.315(11)	0.0262(16)
	Ga	G_3	24*d*	0.0480(3)	0.2590(3)	0.0515(2)	0.73(3)	0.034(4)
	Pd S[a]	P_3	24*d*	0.0703(4)	0.2409(3)	0.0655(2)	0.244(17)	0.0122(17)
	Pd	P'_3	24*d*	0.0247(19)	0.281(2)	0.0389(12)	0.026(8)	0.017(9)
	Pd	P''_3	24*d*	0.0946(11)	0.2167(10)	0.0869(10)	0.028(4)	0.012(8)
Icosahedron	Tb	Tb_1	24*d*	0.15257(2)	0.33563(2)	0.26729(2)	1	0.00712(6)
	Tb	Tb_2	24*d*	0.04149(2)	0.15408(2)	0.34227(2)	1	0.00821(6)
	Tb	Tb_3	24*d*	0.03748(2)	0.34490(2)	0.47105(2)	1	0.00786(6)
	Tb	Tb_4	8*c*	0.46049(2)	0.46049(2)	0.46049(2)	1	0.00794(10)
	Tb	Tb_5	24*d*	0.27219(2)	0.34569(2)	0.46669(2)	1	0.01022(7)
Icosidodecahedron	Ga	G_5	24*d*	0.24957(3)	0.28809(3)	0.35140(3)	1	0.00986(14)
	Ga	G_6	24*d*	0.08683(3)	0.46557(3)	0.43929(3)	1	0.00970(14)
	Ga	G_7	24*d*	0.13360(3)	0.41070(3)	0.15624(3)	1	0.01157(15)
	Ga	G_8	24*d*	0.21345(3)	0.44986(3)	0.23976(3)	1	0.01088(15)
	Ga	G_9	24*d*	0.15293(3)	0.35258(3)	0.39839(3)	1	0.01131(14)
	Ga	G_{11}	24*d*	0.06003(3)	0.28574(3)	0.35412(3)	1	0.01172(15)
	Ga	G_{12}	24*d*	0.22556(4)	0.46872(4)	0.44028(4)	1	0.01663(17)
	Ga	G_{13}	24*d*	0.02868(4)	0.35884(4)	0.23294(4)	1	0.01758(17)
	Ga	G_{14}	24*d*	0.02854(4)	0.36777(4)	0.08628(4)	1	0.01958(18)
	Pd	P_{11}	24*d*	0.0764(8)	0.2150(10)	0.4529(11)	0.84(4)	0.004(4)
RTH	Ga	G_{15}	8*c*	0.35225(3)	0.35225(3)	0.35225(3)	1	0.0086(2)
	Ga	G_{16}	24*d*	0.14724(3)	0.45567(3)	0.33904(3)	1	0.00968(14)
	Ga	G_{17}	24*d*	0.02870(4)	0.47858(4)	0.15906(4)	1	0.01912(18)
	Pd	P_{12}	24*d*	0.24551(2)	0.40255(2)	0.34280(2)	1	0.01027(10)
	Pd	P_{13}	24*d*	0.05127(2)	0.39913(2)	0.34751(2)	1	0.00950(10)
	Pd	P_{14}	24*d*	0.33958(2)	0.44681(2)	0.40967(2)	1	0.01294(11)
	Pd	P_{15}	24*d*	0.09038(3)	0.46338(2)	0.24624(2)	1	0.01390(11)
	Pd	P_{16}	24*d*	0.06428(3)	0.09295(3)	0.46608(3)	0.913(3)	0.015(2)

[a]For simplicity, largely displaced sites on the dodecahedron vertices are denoted as L, while the split sites on the same shell are denoted as S.

feature in Tsai-type compounds, the RTH shell [unit number (4)] is composed of three inner shells [assigned as unit numbers (1) to (3)] surrounding a central unit labeled as a unit (0) in Fig. 4(b). In the refined model shown in Fig. 4, most atomic sites (apart from a small number of disordered positions mostly around the cluster center) are fully occupied by distinct atomic species. Indeed, only 7.40% of atomic sites within one RTH cluster are fractionally occupied, which is exceptional among all the ternary higher-order ACs reported to date. Take Cd-Mg-Y 2/1 AC as an example [28], wherein the percentage of mixed sites within the cluster amounts to ∼73.45%. It seems that very low chemical disorder is a characteristic feature of the present structure. In the following, we discuss structural features of each shell within the RTH cluster starting from the innermost unit.

The core unit, assigned as a unit number (0) in Fig. 4(b), appears in a curious fashion and bears no resemblance to commonly observed central units in Tsai-type or even pseudo-Tsai-type systems, where tetrahedron (either ordered or disordered) and single fully/partially occupied RE atoms are found, respectively [27]. It rather exhibits an orientationally fixed trigonal pyramidlike unit encircled by a few positionally

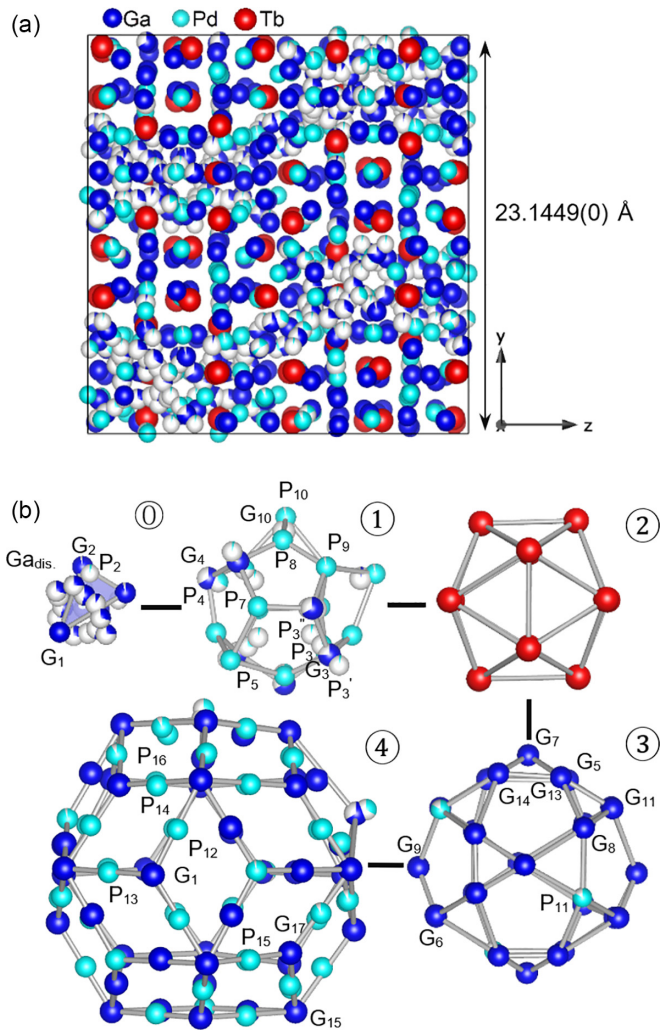

FIG. 4. (a) Atomic decoration within a unit cell of the $Ga_{50}Pd_{35.5}Tb_{14.5}$ 2/1 approximant crystal (AC) with a lattice parameter of 23.1449(0) Å. (b) The successive sequence of atomic shells; the inner most unit labeled as (0) wherein orientationally fixed trigonal pyramidlike unit encircled by a few translationally disordered Ga atoms, denoted as $Ga_{dis.}$ atoms, is noticed. The outer shells surrounding the central unit are (from the closest shell to the central unit): significantly deformed Ga/Pd dodecahedron, a Tb icosahedron, a Ga/Pd icosidodecahedron and a Ga/Pd rhombic triacontahedron (RTH).

disordered atoms around its midheight, which are referred to as $Ga_{dis.}$ throughout this paper. Figure 5 provides a clearer illustration of the electron density distribution at the center of the cluster by indicating the electron densities on the three cut planes perpendicular to the [111] axis labeled as 1, 2, and 3, which are normal to the bisecting plane of an isovolume electron density cube shown in the bottom-left corner of Fig. 6(b). Plane numbers 1, 2, and 3 pass through a tip, a midheight, and a base triangle of the pyramid, respectively. Clearly, there are four strong localized electron densities at the vertices of the trigonal pyramidlike unit and some smeared off-plane densities with lower intensities around its midheight. The base of the pyramid is an equilateral triangle with a length of 3.0324(2) Å, while its height and slant distances amount to

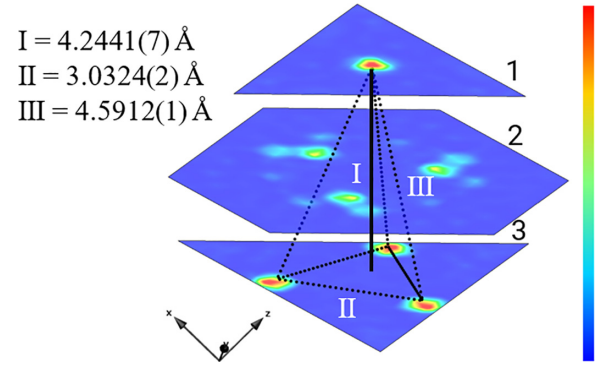

FIG. 5. The electron densities on the three cut planes normal to the [111] axis labeled 1, 2, and 3 passing through a tip, a midheight, and a base triangle of the trigonal pyramid, respectively.

4.2441(7) and 4.5912(1) Å, respectively. Notice the long pyramid height that exceeds the typical bond lengths between Ga and/or Pd pairs which lie in a range of 2.50–2.69 Å [42]. It can be assumed that $Ga_{dis.}$ appear to fill the extra space generated by the elongated trigonal pyramid and yet find it difficult to be stabilized due to extremely compact atomic environment. Note that the centerline of the trigonal pyramid coincides with threefold axes of the unit cell. Whether such orientational ordering at the cluster center takes part in AFM order establishment in the present sample is unclear. In the AFM Cd_6RE 1/1 ACs wherein the cubic symmetry breaks below a certain temperature due to the Cd_4 tetrahedra ordering, it has been proposed that the distortion of the icosahedra modifies the magnetic exchange interactions and induces the magnetic ordering possibly due to the relief of some frustration inherent to the perfect icosahedron or octahedron arrangement of RE [43]. The same approach has also been taken elsewhere [30]. The reason for the structural distortion in the Cd_6RE 1/1 ACs is that the cubic symmetry cannot be retained after the orientational ordering of Cd_4 tetrahedra, and thus, the structure transforms to a monoclinic [44].

Based on the above discussion, it is crucial to explore whether the orientational ordering of the cluster center in the present compound is compatible with the symmetry constraints posed by the space group $Pa\bar{3}$. Figures 6(a)–6(c) provide spatial distribution of the isolated trigonal pyramids within a unit cell viewed along main zone axes. The red vectors represent [111] and equivalent directions. The *a*-glide planes and the symmetry centers (or inversion points) at (0 0 0), (½ 0 0), (½ ½ 0), (0 ½ 0), and (½ ½ ½) associated with the space group $Pa\bar{3}$ are also shown in Fig. 6. Clearly, unlike 1/1 ACs, the center of cubic symmetry in the 2/1 AC does not coincide with the center of the RTH cluster, and thus, the distribution of trigonal pyramids, the tips of which always point toward ⟨111⟩ direction, perfectly follows the symmetry constraints posed by the space group $Pa\bar{3}$.

As mentioned earlier, the height and the slant lengths of the pyramid are 4.2441(7) and 4.5912(1) Å, respectively. Allocating a unit with such dimensions especially at the center of a highly compact RTH cluster is expected to have some serious consequences to the whole structure, particularly the surrounding dodecahedron cage. Figure 7 shows the electron density isosurface generated from F_{obs} at the 18 $e/Å^{-3}$ level at

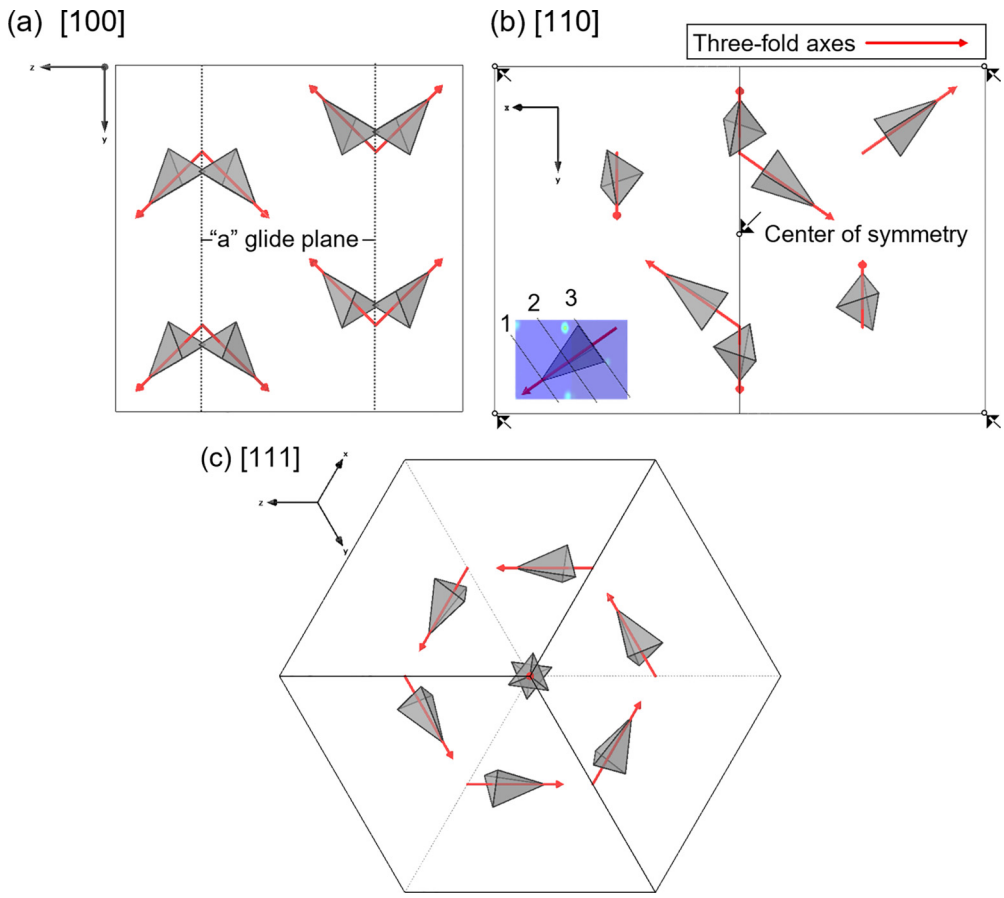

FIG. 6. The distribution of eight trigonal pyramids within one unit cell viewed along (a) [100], (b) [110], and (c) [111] directions. The red vectors that pass through the center of trigonal pyramids in (a)–(c) represent ⟨111⟩ direction.

the center of a cluster including the central unit (represented by red color) and the surrounding dodecahedron. Overall, two consequences can be distinguished on the dodecahedron shell. First is the significant displacement of the four vertices labeled as L sites (atoms P_5 and P_6 in Table II), which seems like a reasonable measure taken to avoid too short interatomic distances between the atoms on the trigonal pyramid and dodecahedron vertices or even their collision. For example, the displacement of the P_5 atom from its ideal position is ∼1.67 Å. Such a displacement allows minimum distances between the trigo-

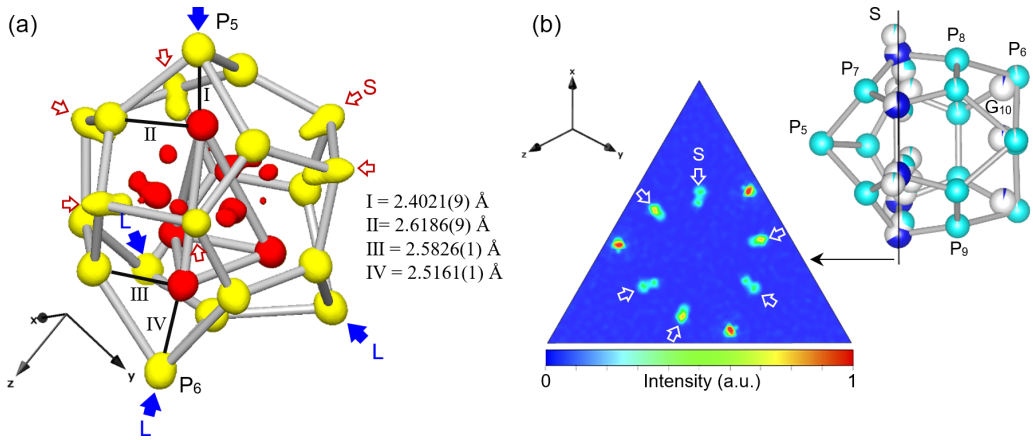

FIG. 7. (a) Electron density isosurface at the cluster core (shown in red) and the deformed dodecahedron (shown in yellow) generated from F_{obs} at 18 $e/Å^{-3}$ level. The blue filled arrows represent four atoms on the dodecahedron vertices that are displaced to avoid too short interatomic distances with the vertices of the triangular pyramid. (b) The two-dimensional (2D) cross-section of the electron density map on the [111] plane wherein the six splitting sites on the dodecahedron vertices are represented by small unfilled arrows. The three unmarked high residual electron density spots in (b) correspond to Tb_5 atoms on the outer shell.

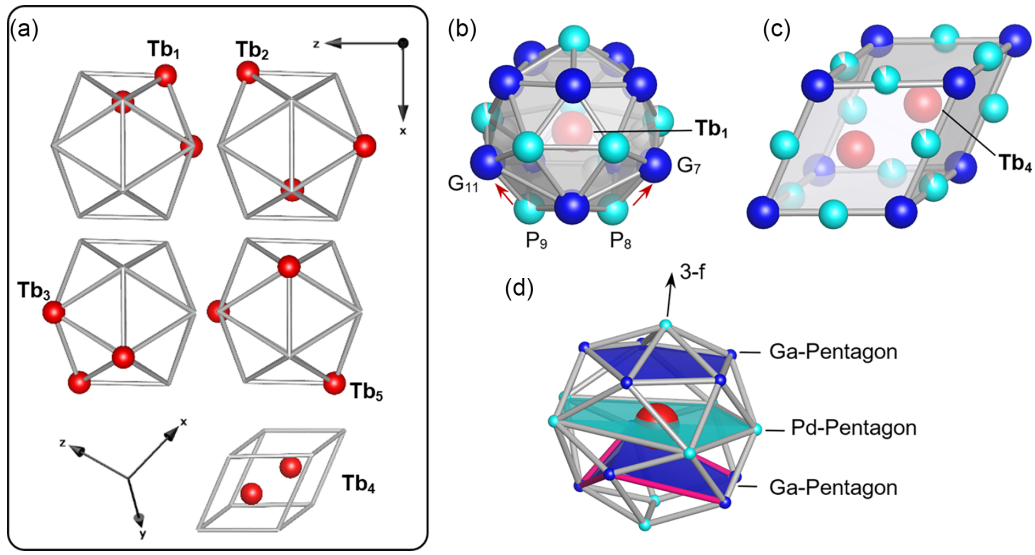

FIG. 8. (a) The Tb atoms with five different Wyckoff positions. Tb_{1-3} and Tb_5 belong to the vertices of the icosahedral shell, while two Tb_4 atoms appear on the long body diagonal axis of the acute rhombohedron (AR). The local structure at the nearest neighbor of an isolated Tb^{3+} ion located at the (b) icosahedron vertices and (c) inside the AR units. The Ga, Pd, and Tb atoms are represented by dark blue, light blue, and red colors, respectively. In (b), the surrounding non-Tb atoms form a $(Ga:Pd)_{18}Tb$ polyhedron with 18 vertices. (d) The same $(Ga:Pd)_{18}$ Tb polyhedron wherein the distortion of one of the three pentagon planes due to the existence of two Pd atoms at the bottom is signified.

nal pyramid and the dodecahedron vertices to be kept in a reasonable range of 2.4021(9) − 2.6186(9) Å. The resultant dodecahedron, therefore, is not a regular but a substantially deformed one. The second noticeable consequence is the site splitting of six atoms on the dodecahedron vertices marked by unfilled red arrows in Fig. 7, hereafter referred to as S sites. These sites, which are better visualized by a cross-sectional two-dimensional (2D) electron density map on the [111] plane in Fig. 7(b), are mixed positions preferentially occupied by Ga with a mixture ratio of $(Ga_{68.5-73} : Pd_{27.2-31.5})$. The appearance of S sites seems to be a natural response of the structure to the presence of $Ga_{dis.}$ atoms around the central pyramid. In other words, the disorder of the $Ga_{dis.}$ atoms extends to the nearest-neighbor atoms on the dodecahedron shell in the form of positional and chemical disorder. The three unmarked high-electron-density spots in Fig. 7(b) correspond to Tb_5 atoms in the outer shell, which will be discussed in the following section. Except six S atoms, the rest of the dodecahedron sites are dominantly occupied by Pd [see Fig. 7(b)].

The second shell from the center, assigned as shell number (2) in Fig. 4(b), is an icosahedron, the vertices of which are fully occupied by four different symmetrically equivalent Tb atoms, as shown in Fig. 8(a). Under the present origin setting, there are additional Tb atoms that appear on a long body diagonal of an AR unit [also shown in Fig. 8(a)] that fills the gap between the RTH clusters at the center of unit cell [see Fig. 1(c) for its schematic illustration]. By taking a different origin setting though, the location of the AR differs in the unit cell, while incidentally, four AR units exist within a unit cell. The local structure around the isolated Tb^{3+} atoms of Tb_1 and Tb_4 types are provided in Figs. 8(b) and 8(c), respectively. In the case of Tb_1, the surrounding non-Tb atoms form a $(Ga:Pd)_{18}$ Tb polyhedron with 18 vertices, 10 of which are preferentially occupied by Ga and the rest by Pd. This polyhedron is slightly different from a $Cd_{16}RE$ monocapped, double, pentagonal antiprismlike polyhedron that forms around RE elements in the Cd_6RE 1/1 ACs [19,20], and the difference lies in the presence of two additional vertices occupied by Pd [P_8 and P_9 in Fig. 8(b)] that push away the two of five Ga atoms [G_7 and G_{11} in Fig. 8(b)] on the vertices of the lower pentagonal plane leading to its out-of-plane distortion, as indicated in Fig. 8(d). On the AR unit encaging the Tb_4 atoms shown in Fig. 8(c), the eight vertices and 12 mid-edges are preferentially occupied by Ga and Pd, respectively. Interestingly, the local environments of Tb^{3+} atoms on either icosahedron shell or inside the AR unit are free from chemical disorder (i.e., free from mixed sites). While such a highly ordered structure around Tb^{3+} atoms reflects structural perfection in the present compound, it is also suggestive of a correlation between the disorder-free environment around Tb^{3+} atoms and the establishment of long-range AFM order in the present compound [29]. Indeed, the adverse effect of chemical disorder on the formation of long-range AFM order in ACs has been demonstrated well by much research [45,46]. A discussion on this subject, however, falls outside the scope of this paper and is left for future studies.

The two outermost shells in Fig. 4(b), denoted as shell numbers (3) and (4), are icosidodecahedron and RTH shells, respectively. In both shells, some degrees of distortion are noticed which seem to originate from a significant distortion of the inner dodecahedron, as discussed earlier. In addition, the atomic sites on both shells, although rarely mixed, are dominantly occupied by either Ga or Pd. Among 30 vertices of an icosidodecahedron shell, 27 are predominantly occupied by Ga, and only three sites, denoted as P_{11} in Table II, are exceptionally resided by Pd. Figure 9 displays superimposed concentric shells and a cross-sectional 2D electron density map on the [13,5,8] plane, where the proximity of the P_{11} site on the icosidodecahedron to the S sites on the dodecahedron (which are dominantly occupied by Ga) is clearly evidenced.

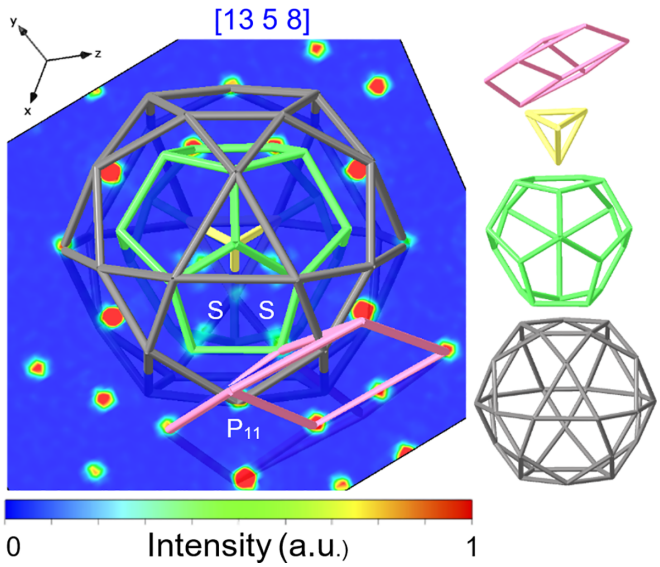

FIG. 9. Cross-sectional two-dimensional (2D) electron density map on [13,5,8] plane passing through a P_{11} site on the icosidodecahedron and the nearest dodecahedron vertices accommodating split S atoms. The figure evidences that the three vertices of the icosidodecahedron, which are exceptionally resided by Pd, locate in a vicinity of the split S atoms on the dodecahedron. The P_{11} site also belongs to the inner midedge of an obtuse rhombohedron (OR) unit drawn in purple.

The physical distance between these two sites by considering the averaged coordination for S atoms amounts to 2.497(9) Å. It seems that the proximity of these two atomic sites changes the occupational preference at the P_{11} position on the icosidodecahedron shell from Ga to Pd. The unit drawn in purple in Fig. 9 will be explained in what follows.

On the outermost RTH shell, denoted as unit number (4) in Fig. 4(b), among the 32 vertices, 26 are fully composed by Ga, three vertices are mixed S sites, and three others are fully resided by Pd. The midedges, on the contrary, are dominantly occupied by Pd and occasionally by Ga. To understand the source of a few inconsistencies in the site occupancies on the RTH shell, it is necessary to consider another building unit called an obtuse rhombohedron (OR). The OR can be described as either a shared section in between two adjacent RTH clusters or a connecting unit of adjacent dodecahedra along threefold axes. As shown in Fig. 10(a), each RTH cluster in the 2/1 AC is connected to surrounding counterparts through six twofold and seven threefold axes (also called *b* and *c* linkages, represented by thick green and yellow bonds, respectively [47]). Along the *c* linkages, the two RTH units are interpenetrated and share sections in the shape of an OR. Another and perhaps more efficient way to describe ORs is to consider them as connecting units of adjacent dodecahedra along *c* linkages, as shown in Fig. 10(b). This way, two types of ORs denoted as OR_I and OR_{II}, represented respectively by blue and red polyhedra in Fig. 10, can be distinguished. The two ORs differ in their atomic arrangement and tip-to-tip length (l). The l in OR_I and OR_{II} equals 3.04 and 2.85 Å, respectively. Shorter l in OR_{II} indicates that it is rather more compressed than OR_I along its height simply because both its tips are occupied by P_5 atoms, which correlate to the largely displaced dodecahedron vertices, denoted as L in Fig. 7. In OR_I, however, one tip corresponds to the L site, while the other one correlates to splitting S sites. Since the center of OR_{II} always coincides with the inversion points associated with the space group $Pa\bar{3}$ at (0 0 0), (½ 0 0), (½ ½ 0), (0 ½ 0), and (½ ½ ½), the atoms on each face of the OR_I are inverted through its center. Each RTH shell is composed of seven ORs, six of which are of type I, and only one is of type II. One can easily notice that all the positions on the RTH shell whose occupancies are inconsistent with the rest of the RTH sites are, indeed, those that belong to OR_I and OR_{II} units. Simply put, the chemical and positional disorder of some atomic sites on the dodecahedron shell affect the occupational

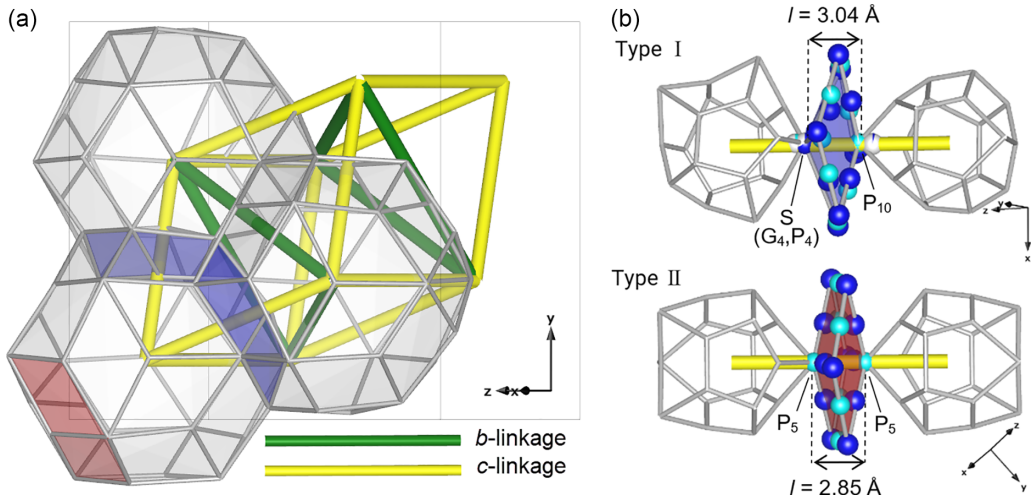

FIG. 10. (a) The arrangement of three rhombic triacontahedron (RTH) clusters within a unit cell connecting through *b* and *c* linkages represented by thick green and yellow bonds, respectively. Along the *c* linkages, the two RTH units are interpenetrated and share sections in the shape of obtuse rhombohedron (OR). (b) Another illustration of ORs as connecting units of adjacent dodecahedra along *c* linkages. Two types of ORs differing in their atomic arrangement and tip-to-tip length (l) can be distinguished. Six out of seven ORs around each decahedron are of type I, while only one is of type II.

preferences of the atomic sites on their interconnecting OR units, which are also shared sections of neighboring RTH units. In terms of directions for future research, it will be interesting to explore possibility of eliminating $Ga_{dis.}$ atoms around an orientationally ordered central units and obtain almost defect-free structure in the ternary system. Optimizing the elemental composition and heat treatment procedure during the synthesis are possible approaches in this direction.

IV. CONCLUSIONS

This paper was undertaken to investigate atomic structure of the AFM Ga-Pd-Tb 2/1 approximant to QC by means of SCXRD at room temperature. This compound is interesting because it is the only higher-order approximant with AFM order which has a relatively high electron density ($e/a = 1.93$), where frustrated magnetic states such as spin-glass are expected. In this paper, special focus was given to any uncommon structural aspects which could possibly contribute to the AFM order establishment in this compound. The structure analysis unveiled extremely low chemical disorder, as the fractionally occupied atomic sites amounted to only 7.40% of the atomic sites in the whole structure. Such trivial chemical disorder is quite exceptional among other ternary higher order ACs. Within a nearest neighbor of an isolated Tb^{3+} ion, a disorder-free environment was noticed, which is presumably one of the main contributors to enhancing AFM order in the present compound. Moreover, an orientationally ordered trigonal pyramidlike unit was discovered at the center of a multishell polyhedron, known as a RTH cluster, marking an observation of such in higher-order approximants. It is believed that the ordering brings structural distortion, which might be sufficient to partially relieve geometrical magnetic frustration and favor long-range magnetic order. Furthermore, the surrounding dodecahedron cage of the central unit is found to be significantly distorted, particularly on its four vertices close to trigonal pyramid vertices. It was shown that the occupational preferences of atomic sites on OR units are highly affected by the chemical and positional disorders of neighboring dodecahedron sites. Taken together, the present results offer valuable insights into possible atomic scale tuning approaches to obtain AFM order in the higher-order approximants or even QCs. The combination of highly ordered structure and some levels of structural distortion seem to serve as key components in developing AFM order in the inherently frustrated Tsai-type compounds.

ACKNOWLEDGMENTS

This paper was supported by Japan Society for the Promotion of Science through Grants-in-Aid for Scientific Research (Grants No. JP19H05817, No. JP19H05818, No. JP19H05819, and No. JP21H01044) and JST, CREST Grant No. JPMJCR22O3, Japan.

[1] D. Shechtman, I. Blech, D. Gratias, and J. W. Cahn, Phys. Rev. Lett. **53**, 1951 (1984).
[2] A. L. Mackay, Acta Cryst. **15**, 916 (1962).
[3] K. H. Kuo, Sci. Cryst. Struct. Highlights Cryst. **13**, 43 (2015).
[4] G. Bergman, J. L. T. Waugh, and L. Pauling, Acta Cryst. **10**, 254 (1957).
[5] R. Berthold, M. Mihalkovic, U. Burkhardt, Y. Prots, A. Amarsanaa, and G. Kreiner, Intermetallics **53**, 67 (2014).
[6] A. Palenzona, J. Less-Common Met. **25**, 367 (1971).
[7] R. Maezawa, S. Kashimoto, and T. Ishimasa, Philos. Mag. Lett. **84**, 215 (2004).
[8] A. P. Tsai, J. Q. Guo, E. Abe, H. Takakura, and T. J. Sato, Nature (London) **408**, 537 (2000).
[9] H. Takakura, C. P. Gómez, A. Yamamoto, M. De boissieu, and A. P. Tsai, Nat. Mater. **6**, 58 (2007).
[10] A. I. Goldman and R. F. Kelton, Rev. Mod. Phys. **65**, 213 (1993).
[11] C. P. Gomez and S. Lidin, Angew. Chem. Int. Ed. **40**, 4037 (2001).
[12] A. P. Tsai, Acc. Chem. Res. **36**, 31 (2003).
[13] A. P. Tsai, Sci. Technol. Adv. Mater. **9**, 013008 (2008).
[14] A. P. Tsai, Chem. Soc. Rev. **42**, 5352 (2013).
[15] W. Steurer and S. Deloudi, Acta Cryst. **A64**, 1 (2008).
[16] K. Inagaki, S. Suzuki, A. Ishikawa, T. Tsugawa, F. Aya, T. Yamada, K. Tokiwa, T. Takeuchi, and R. Tamura, Phys. Rev. B **101**, 180405(R) (2020).
[17] Y. So, A. Katagiri, R. Tamura, and K. Edagawa, Philos. Mag. Lett. **98**, 292 (2018).
[18] T. Yamada, Y. Nakamura, T. Watanuki, A. MacHida, M. Mizumaki, K. Nitta, A. Sato, Y. Matsushita, and A. P. Tsai, Inorg. Chem. **58**, 9181 (2019).
[19] C. P. Gómez and S. Lidin, Phys. Rev. B **68**, 024203 (2003).
[20] M. Armbruster and S. Lidin, J. Alloys Compd. **307**, 141 (2000).
[21] F. Labib, N. Fujita, H. Takakura, S. Ohhashi, T. Shiino, A. P. Tsai, and R. Tamura, J. Alloys Compd. **954**, 170151 (2023).
[22] C. P. Gûmez and S. Lidin, Chem. Eur. J. **10**, 3279 (2004).
[23] R. Tamura, Y. Murao, S. Takeuchi, M. Ichihara, M. Isobe, and Y. Ueda, Jpn. J. Appl. Phys. **41**, L524 (2002).
[24] R. Tamura, Y. Muro, T. Hiroto, K. Nishimoto, and T. Takabatake, Phys. Rev. B **82**, 220201(R) (2010).
[25] T. Kong, S. L. Budko, A. Jesche, J. McArthur, A. Kreyssig, A. I. Goldman, and P. C. Canfield, Phys. Rev. B **90**, 014424 (2014).
[26] G. Gebresenbut, T. Shiino, D. Eklöf, D. C. Joshi, F. Denoel, R. Mathieu, U. Häussermann, and C. Pay Gómez, Inorg. Chem. **59**, 9152 (2020).
[27] G. H. Gebresenbut, R. Tamura, D. Eklöf, and C. P. Gómez, J. Phys.: Condens. Matter **25**, 135402 (2013).
[28] T. Yamada, N. Fujita, and F. Labib, Acta Cryst. **B77**, 638 (2021).
[29] Y. G. So, K. Takagi, and T. J. Sato, J. Phys.: Conf. Ser. **1458**, 012003 (2020).
[30] F. Labib, H. Takakura, A. Ishikawa, and R. Tamura, Phys. Rev. Mater. **6**, 124412 (2022).
[31] A. Jagannathan, Phys. Rev. Lett. **92**, 047202 (2004).
[32] S. Thiem and J. T. Chalker, Phys. Rev. B **92**, 224409 (2015).
[33] S. Matsuo, S. Fujiwara, H. Nakano, and T. Ishimasa, J. Non. Cryst. Solids **334-335**, 421 (2004).
[34] E. Y. Vedmedenko, U. Grimm, and R. Wiesendanger, Phys. Rev. Lett. **93**, 076407 (2004).

[35] S. Thiem and J. T. Chalker, Europhys. Lett. **110**, 17002 (2015).
[36] C. Godréche, J. M. Luck, and H. Orland, J. Stat. Phys. **45**, 777 (1986).
[37] R. Lifshitz, Phys. Rev. Lett. **80**, 2717 (1998).
[38] G. M. Sheldrick, Acta Cryst. A **71**, 3 (2015).
[39] G. M. Sheldrick, Acta Cryst. C **71**, 3 (2015).
[40] A. Le Bail, H. Duroy, and J. L. Fourquet, Mat. Res. Bull. **23**, 447 (1988).
[41] V. Petrícek, M. Dušek, and L. Palatinus, Z. Kristallogr. Cryst. Mater. **229**, 345 (2014).
[42] Y. R. Luo, *Comprehensive Handbook of Chemical Bond Energies* (CRC Press, Boca Raton, 2007).
[43] M. G. Kim, G. Beutier, A. Kreyssig, T. Hiroto, T. Yamada, J. W. Kim, M. de Boissieu, R. Tamura, and A. I. Goldman, Phys. Rev. B **85**, 134442 (2012).
[44] R. Tamura, K. Edagawa, K. Shibata, K. Nishimoto, S. Takeuchi, K. Saitoh, M. Isobe, and Y. Ueda, Phys. Rev. B **72**, 174211 (2005).
[45] T. Hiroto, T. J. Sato, H. Cao, T. Hawai, T. Yokoo, S. Itoh, and R. Tamura, J. Phys.: Condens. Matter **32**, 415802 (2020).
[46] P. Das, P. F. Lory, R. Flint, T. Kong, T. Hiroto, S. L. Bud'ko, P. C. Canfield, M. de Boissieu, A. Kreyssig, and A. I. Goldman, Phys. Rev. B **95**, 054408 (2017).
[47] C. P. Gómez and A. P. Tsai, Comptes Rendus Phys. **15**, 30 (2014).